Enhancement of magnetic properties in compressively-strained $PrVO_3$ thin films

D. Kumar,[1] A. Fouchet,[1] A. David,[1] A. Cheikh,[1]
O. Copie,[2] C. U. Jung,[3] A. Pautrat,[1] W. Prellier[1*]
[1]*Laboratoire CRISMAT, CNRS UMR 6508,*
ENSICAEN, Normandie Université,
6 Bd Maréchal Juin, F-14050 Caen Cedex 4, France
[2]*Institut Jean Lamour, UMR 7198,*
CNRS/Université de Lorraine, 54011 Nancy, France and
[3]*Department of Physics, oxide research center,*
Hankuk University of Foreign Studies, Yongin, Gyeonggi 17035, Korea

Abstract

Strain engineering is an important issue in oxides thin films to explore new functionalities. Here, a series of high quality epitaxial $PrVO_3$ (PVO) thin films were grown, by Pulsed Laser Deposition (PLD) technique, as a function of thickness on (La,Sr)(Al,Ta)O_3 (100) [LSAT (100)] and $LaAlO_3$ (100) [LAO (100)] substrates with nominal lattice mismatch of -0.8 % and -2.9 %, respectively. The X-ray diffraction revealed a constant *out-of-plane* lattice parameter of PVO/LSAT with increase in film thickness, while a rather continuous decrease for PVO/LAO films. Whereas thicker PVO films show a ferromagnetic-like behavior, at low thickness a surprising decrease of coercivity (H_c) and increase of saturation magnetization (M_s) is observed. This behavior is described using a classical model of "dead layer" which possesses a strong paramagnetic susceptibility. It is also shown how capping of PVO film can aid in recovering the pure magnetic properties of PVO, by diminishing the contribution from "dead layer". Finally, the Néel temperature (T_N) is examined as a function of film thickness, and found to vary in the range of 25 K and 30 K for LSAT and LAO, respectively. These results pave the way for the use of vanadate in thin film devices.

PACS numbers: 81.15.Fg, 73.50.Lw, 68.37.Lp, 68.49.Jk

*wilfrid.prellier@ensicaen.fr

I. INTRODUCTION

The perovskite oxides with generic formula ABO_3 have attracted a great deal of scientific interest thanks to the strong correlation between orbital (electronic), spin (magnetic) and lattice degrees of freedom (structural). Consequently, owing to various functional properties such as ferroelectricity, ferromagnetism, antiferromagnetism, colossal magnetoresistance, superconductivity, the oxides are exploited in the diverse technological applications for electronics, data storage or sensing and so on [1–4]. While for bulk materials, these underlying properties can be expanded via lattice distortion by applying hydrostatic pressure [5, 6], a substrate-induced biaxial strain in ABO_3 epitaxial thin films proved to be an effective tool to modify the spin-orbit-lattice coupling [7–10]. Among RVO_3 (R: Rare earth element), the bulk $PrVO_3$ (PVO), at room temperature, adopts an orthorhombic $Pbnm$ crystal structure with the lattice parameters: $a_o = 5.487$ Å, $b_o = 5.564$ Å, and $c_o = 7.778$ Å (o stands for orthorhombic) [11]. In the following, we will consider the pseudocubic unit cell of PVO that yields $a_{pc} \approx a_o/\sqrt{2} \approx b_o/\sqrt{2} \approx c_o/2 \approx 3.901$ Å (pc stands for pseudocubic). The bulk PVO is an antiferromagnet associated with C-type Spin Ordering (C-SO), where V spins are staggered in ab-plane and aligned ferromagnetically along the c-axis, with $T_N \simeq 130$ K [12]. However, for a PVO thin film, the DFT calculations reveal a G-type Spin Ordering (G-SO) in the ground state (where V spins are aligned antiferromagnetically along all three crystal directions), associated with a C-type Orbital Ordering (C-OO) through Kugel–Khomskii mechanism [13, 14]. In the course of our previous study, we revealed a new pathway to tune the magnetic properties of PVO thin films grown on $SrTiO_3$ (STO) substrate by monitoring the concentration of oxygen vacancies in PVO films [13]. A careful crystal structural investigation revealed that the tensile-strained PVO film on STO substrate adopts a monoclinic $P2_1/m$ crystal lattice [10, 13, 15]. In addition, we have scrutinized the effect of substrate-induced strain on the structural and magnetic properties, by growing PVO films on top of various lattice mismatched perovskite-oxide substrates [10]. The study revealed that a large compressive strain in PVO films not only promotes the superexchange interaction *i.e.* V–V interactions, but also changes the electronic structure of PVO. Recent investigations have unveiled that the layer-by-layer control of film through minute deposition tunes the strain states in a film, offering fascinating functional properties, namely, spin-glass behaviour in compressively strained $BiFeO_3$ thin films [16], thickness dependent magnetic anisotropy in

$La_{2/3}Ca_{1/3}MnO_3$ films [17] and the dimensional crossover of magnetization from 3D to 2D in $SrRuO_3$ thin films with decrease in film thickness [18]. Even if the RVO_3 system is a good candidate to exhibit the spin-orbit-lattice coupling, only a few film thickness-dependence studies have been conducted in thin films [19, 20].

In this paper, we study the thickness-dependent structural and magnetic properties of the $PrVO_3$ (PVO) thin films grown on (La,Sr)(Al,Ta)O_3 (LSAT) and $LaAlO_3$ (LAO) substrates. While thick PVO films (100 nm) remain strained to the LSAT substrates, films of $\sim$ 50 nm show partial relaxation on the LAO substrates. We have evidenced a dead-layer at the film surface which possesses strong paramagnetic susceptibility, and is at the origin of observed magnetic properties. In addition, we have also explored the possibility to heal this layer by capping with few layers of LAO, in order to recover the magnetic properties of PVO.

II. EXPERIMENTAL

The PVO thin films were epitaxially grown on top of (100)-oriented LAO and LSAT substrates, within thickness range of 10 to 100 nm, by using Pulsed Laser Deposition (PLD) technique. A KrF excimer laser (λ = 248 nm) with repetition rate of 2 Hz and laser fluence of 2 J/cm^2 was focused on a $PrVO_4$ ceramic target, with substrate-to-target distance of 5 cm. The films were deposited at a growth temperature T_G = 650 °C and oxygen partial pressure $P_{O_2} = 10^{-6}$ mbar. To assure homogeneous oxygen vacancies throughout the growth, the samples were cooled down to room temperature in the same oxygen pressure. The crystallinity and the structure of the PVO films were characterized using x-ray diffraction technique (Bruker D8 Discover diffractometer, Cu $K\alpha 1$ radiation, λ = 1.5406 Å). The surface morphology of the films was investigated using Atomic Force Microscopy (AFM) PicoSPM. The magnetic measurements were performed using Superconducting Quantum Interference Device (SQUID) magnetometer, as a function of magnetic field H (parallel configuration) and temperature T. The magnetization-magnetic field (M-H) hyteresis curves were obtained at T = 20 K and magnetization-temperature (M-T) data were carried out at $H_{in-plane}$ = 50 Oe. The lattice constants of PVO, LSAT, and LAO in the *pseudo-cubic* structure are 3.901 Å, 3.868 Å, and 3.791 Å respectively, establishing PVO to be grown under nominal compressive strain with lattice mismatch of -0.8 % (LSAT) and -2.9 % (LAO).

III. RESULTS AND DISCUSSION

Figure 1(a) and 1(b) display θ - 2θ x-ray diffraction measurements of a series of PVO films grown on top of (100)-oriented LAO and LSAT substrates respectively, around $(100)_{pc}$ (where *pc* refers to the *pseudo-cubic* notation) of each substrate. The clear thickness fringes for PVO/LSAT films confirm uniform thickness, and well-defined film/substrate interface. However, PVO films grown on LAO substrates display suppressed oscillations, presumably due to presence of the twin domains in the LAO substrate [21]. The film thickness (t) was calculated using these fringes, the details of which could be found elsewhere [10]. The AFM analysis was performed on each sample, and a surface roughness less than 0.5 nm was observed confirming the high-quality of the samples, without the presence of any islands even in the thicker films (Fig. 1(d)). The *out-of-plane* and *in-plane* lattice parameters were calculated using XRD θ - 2θ (Fig. 1(a), (b)) and reciprocal space map scans (Fig. 2), respectively.

Figure 1(c) illustrates the evolution of PVO lattice parameters as a function of the film thickness, for both LAO and LSAT substrates. First, we see that the *out-of-plane* lattice parameter of all PVO films has increased for both substrates as compared to that of the *pseudo-cubic* bulk PVO (solid red line in Figure 1(c)), which is in perfect agreement with the *in-plane* compressive strain imposed by the LAO and LSAT substrate. Moreover, the *out-of-plane* lattice parameter of PVO/LAO decreases continuously (in overall) with increase of film thickness, although a slight increase between $t = 19.63$ nm and $t = 24.19$ nm, and also between $t = 55.93$ nm and $t = 74.50$ nm is observed, and believed to be because of uncertainty in the calculations of parameters. Second, PVO films grown on the LSAT substrates show a nearly constant *out-of-plane* lattice parameter with increase of film thickness, and a slight change is within the experimental accuracy. (The error bars were calculated by fitting the film peak using the Voigt function, and then using the relation between the uncertainty in lattice parameter (Δd) and Bragg's angle ($\Delta\theta$): $\Delta d = \frac{\Delta\theta}{\tan\theta} \cdot d$, directly derived from the Bragg diffraction expression). This nearly constant behavior of *out-of-plane* lattice parameter of PVO film on LSAT substrate can be rather anticipated due to a smaller mismatch between PVO and LSAT substrate ($\sim$ -0.8 %).

In order to further investigate the thickness-dependent structural evolutions, the asymmetrical reciprocal space maps (RSMs) were recorded for PVO films, around $(103)_{pc}$ Bragg's peak

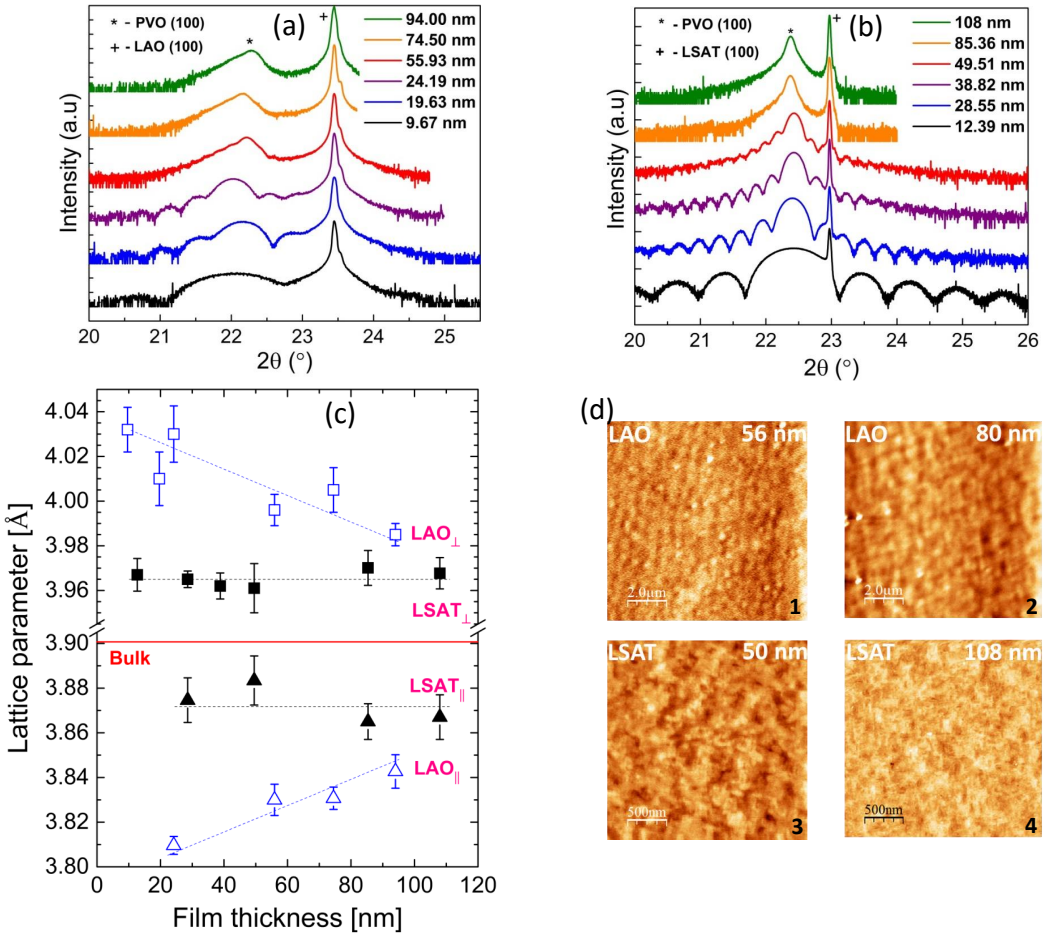

Figure 1: θ - 2θ x-ray diffraction measurements of a series of PVO films grown on (a) LAO and (b) LSAT substrates, around $(100)_{pc}$ of each substrate. The asterisk ($*$) and plus ($+$) represents PVO film and substrate, respectively. (c) *Out-of-plane* (square symbols in top panel) and *in-plane* (triangle symbols in bottom panel) lattice parameters of PVO films grown on LAO (blue open symbols) and LSAT (black close symbols) substrates, as a function of the film thickness, plotted along with the error bars. $\perp$ and $||$ symbols represent the *out-of-plane* and *in-plane* lattice parameters of PVO, respectively. The dashed lines serve as guide to the eyes. Red line indicates PVO bulk *pseudo-cubic* lattice parameter. (d) Representative AFM images of PVO thin films grown on LAO (10x10 μm^2) and LSAT (2.5x2.5 μm^2) substrates. Different thicknesses are shown. The surface roughness (R_q) from 1 to 4 is: 0.18 nm, 0.43 nm, 0.22 nm and 0.42 nm, respectively.

of LAO and LSAT (see Figure 2(a) and 2(b) for PVO/LAO and PVO/LSAT, respectively). We note that the thinner PVO film ($t \leq 24$ nm) is *in-plane* strained when grown onto LAO, whereas thicker films start to relax (Figure 2(a)), as the position of films peak along the

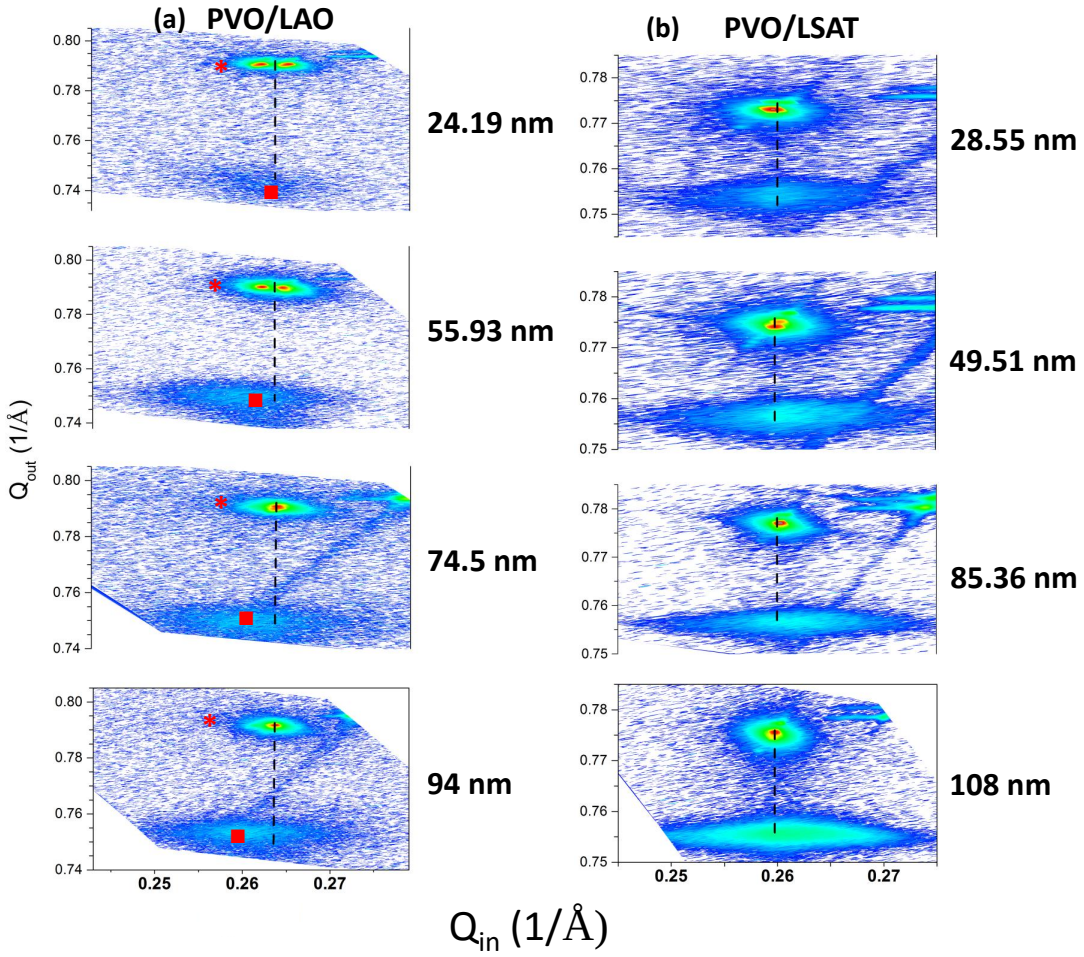

Figure 2: Asymmetrical Reciprocal Space Maps (RSMs) performed for a series of PVO thin films grown on (a) LAO and (b) LSAT substrate, around *pseudo-cubic* (103) of the substrate. The horizontal axis is Q_{in} and vertical axis is Q_{out} for all RSMs. The substrate and film peaks are located in the upper and lower region of RSMs, and marked by the asterisks and solid square symbols respectively, for both substrates. The double peaks for the LAO substrate are due to twin domains in the substrate. The vertical dashed lines are only guide to the eyes.

horizontal Q_{in} axis shifts toward lower value. This is in perfect agreement with the highly mismatched PVO films grown on the LAO substrate which tend to relax easily over small thickness, due to a decrease in the strain states as the thickness increases. The *in-plane* lattice parameters of PVO were calculated using these maps (within the instrumental error) (Fig. 2), and the results are plotted as a function of film thickness in Figure 1(c). On the LAO substrate, the *in-plane* lattice parameter of film increases linearly with the film

thickness. This behavior is typical of a partially relaxed films, and is in accordance with the decrease of *out-of-plane* lattice parameter with increase in film thickness, for a film with an ideal Poisson's ratio [27]. On the LSAT substrates, the situation is different as the PVO films are strained with the substrate, even at $t \sim 100$ nm. This is clearly seen in Figure 2(b) where the horizontal position of film peak coincides with the one of LSAT substrate. Thus, the film and substrate have same *in-plane* lattice parameter. Also, the film peak width along q_{in}-axis increases slightly with increase of film thickness, and could be possibly due to the presence of different domains in the PVO film, as shown in the earlier reports [10, 13, 15]. Moreover, a range of film thickness analyzed by using electron microscopy [10] in combination with pole figures yield PVO $[001]_o$-axis along in-plane of film, and thus inducing $[110]_o$-axis growth. A detailed microstructure of the films will be published later. To summarize, the PVO films are strained when grown on the LSAT substrates, even at $t \sim 100$ nm, whereas films of $t \geq 50$ nm display partial relaxation when grown on LAO substrates.

Figure 3 details the magnetization-magnetic field (M-H) measurements recorded at $T = 20$ K. In order to clearly observe the PVO magnetic contribution, the diamagnetic signals of the substrates were subtracted from the total measured signal. The magnetic hysteresis cycles for the selected PVO samples are shown in Figure 3(a), (b) for LAO substrate and Figure 3(e), (f) for LSAT substrate. A clear opening of the hysteresis loop is observed with increase in the film thickness, evidencing a low temperature ferromagnetic-like behavior of the PVO films. The magnetic moments are however canted, leading to a canted-antiferromagnetic state via antisymmetric spin-spin interaction ($D_{ij}.(S_i \times S_j)$, with D_{ij} the Dzyaloshinskii–Moriya term) [15]. Additionally, the magnetization of PVO films could be described as combination of a soft and a hard magnetic phase, similar to what was observed in orthoferrite $YFeO_3$ [22, 23], and is consistent with our previous observations [10]. In fact, we have shown earlier that the weightage of each magnetic phase can be tuned by the epitaxial strain imposed by different substrates [10]. In the present case, where strain is induced via different thicknesses, we observed a decreasing trend of soft magnetic phase with increase of film's thickness. From Figure 3(a), (b) for PVO/LAO and 3(e), (f) for PVO/LSAT, we extract that, the thinner films indeed posses a larger soft magnetic phase (paramagnetic) with large saturation magnetization (M_s), and with the increase of film thickness, the fraction of film that is made up of paramagnetic phase reduces, and / or the relative contribution of PVO layer, associated with hard magnetic phase, increases. Moreover, we have shown previously

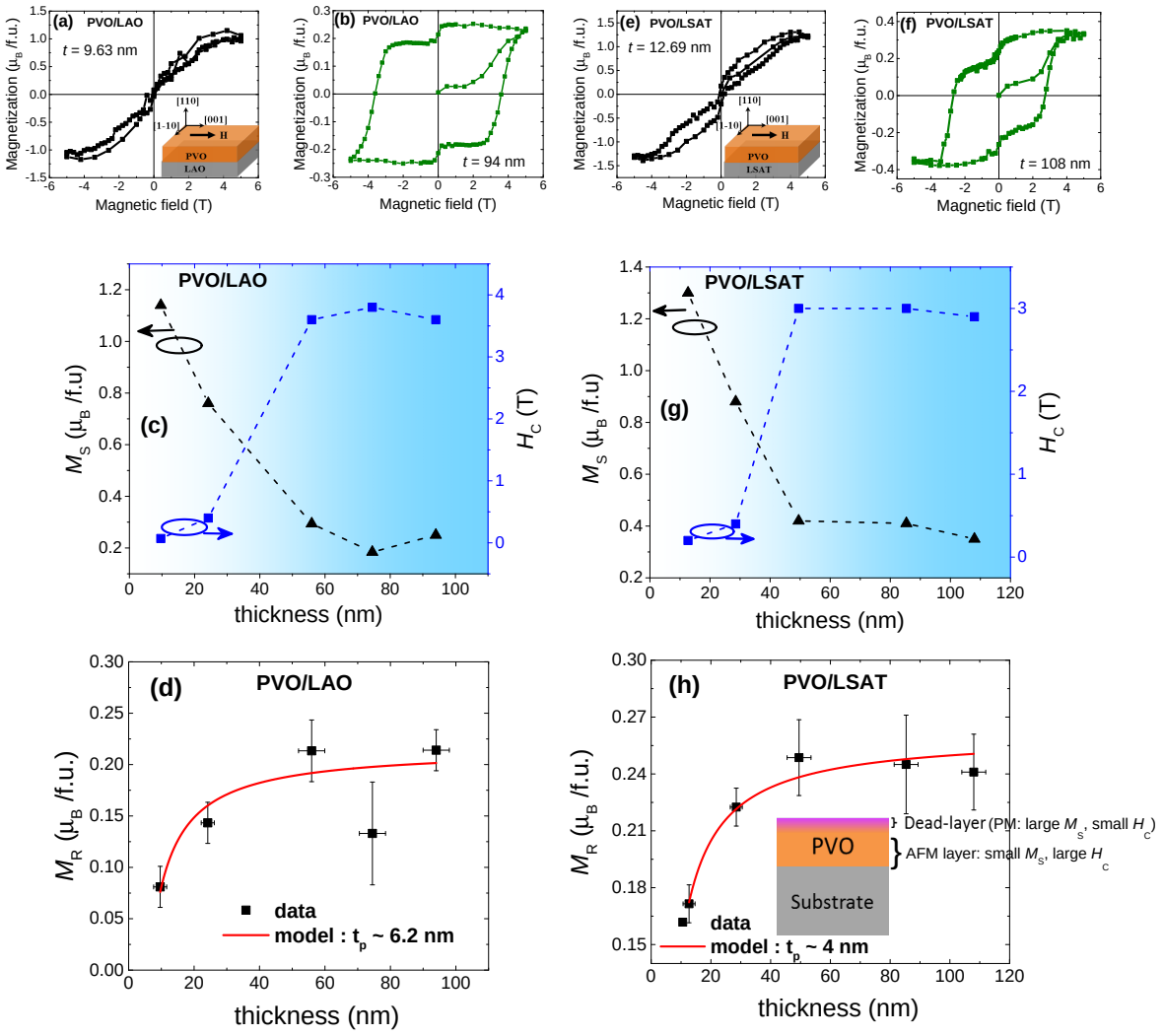

Figure 3: Magnetization (M) vs *in-plane* magnetic field (H) measurements obtained at 20 K for: PVO films grown on (001)-oriented LAO substrate, for film thickness (a) t = 9.63 nm and (b) t = 94 nm, and for PVO/LSAT films (e) t = 12.69 nm, (f) t = 108 nm. Plot of the saturation magnetization (M_s) (left scale) and magnetic coercivity (H_c) (right scale) as a function of the film thickness for (c) PVO/LAO, and (g) PVO/LSAT films. The shaded area represents thickness range where M_s and H_c almost freeze and does not change with film thickness. Thickness-dependence of the remanent magnetization (M_R) for (d) PVO/LAO, and (h) PVO/LSAT films. The red line is a fit to M_R vs. t plot, using equation (2). The right down-inset in (a),(e) represents schematic of magnetization measurements, where the directions refer to the orthorhombic symmetry of PVO. The inset of (h) is a scheme of dead-layer on the surface of film. The dashed lines are only guide for the eyes.

that the soft magnetic component also depends upon the temperature, namely, it disappears at temperature $T > 20$ K for PVO/LSAT, and $T > 80$ K for PVO/LAO films of $t \sim 50$ nm[10]. We will come back to this later in the MT section. The magnetic coercivity (H_c), extracted from the hysteresis loops (hard magnetic phase) and the M_s are plotted as a function of film thickness (See Figure 3(c) for LAO and Figure 3(g) for LSAT). A continuous decrease in M_s and increase in H_c are observed for both the substrates with increase in the film's thickness, until a nominal value is reached, which remain nearly constant for thick films. Additionally, the shape of hysteresis loop changes from a square like MH to a paramagnetic like S-shaped as thickness is reduced. Here, we suggest that a large value of M_s for thinner films is reminiscent of the presence of a non-magnetic/paramagnetic layer at the surface of film, namely a "dead layer", similar to the previous observation in $DyTiO_3$ thin films [25]. When the film surface is exposed to air, the surface can get over-oxidized, and the magnetic V^{3+} ions can indeed be replaced by V^{4+}/V^{5+} (non-magnetic) ions, decoupling Pr^{3+} ions and thus unleashing their strong paramagnetic response. Therefore, the soft magnetic phase is due to presence of the dead layer at the film surface. It is indeed true that a dead layer may also be present at the film/substrate interface [24]. We hypothesize that the layer presents at the surface of film dominates, due to excess oxidation, resulting from air exposure. To estimate the thickness of this layer, we use a model described by equation (1) [25], which assumes that this layer is paramagnetic, has null magnetization at remanence, and a huge magnetization at high fields. We then fit the thickness-dependence of remanent magnetization (M_R) and saturation magnetization (M_s) with the proposed dead layer model, using the following equation:

$$M_{tot.} = m_{tot.}t = m_P t_P + m_{AF} t_{AF} \tag{1}$$

$$m_{tot.} = (m_P - m_{AF})t_P/t + m_{AF} \tag{2}$$

where, $t = t_P + t_{AF}$ is the total thickness of film, t_P is the thickness of paramagnetic layer, t_{AF} is the thickness of antiferromagnetic layer, m_P is the moment per unit volume of the paramagnetic layer, m_{AF} is the moment per unit volume of the antiferromagnetic layer. Setting $m_{AF} \sim 0.7\ \mu_B$/f.u. (f.u.: formula unit)[26] (for bulk PVO) and $m_P = 0$ (for M_R), a dead layer thickness t_P of ~ 6 nm for LAO (Figure 3(d)) and ~ 4 nm for LSAT (Figure 3(h)) was obtained by fitting the remanent magnetization. Furthermore, setting m_P to the maximum magnetization of the thinnest sample and using t_P as fitting parameter, we evaluated $t_P \sim$

10–12 nm from fitting of M_s (not shown). The inconsistency in the computation of t_P from fit of M_R–t and M_s–t can have two possible explanations. First, when the diamagnetic substrate contribution is subtracted, there is always some uncertainties concerning M_s. Second, the magnetic moments associated with the paramagnetic layer, which typically consists of isolated Pr^{3+} ions, may not necessarily be saturated at 5T (especially for thinner films), and thus a large error in the calculation of t_P from M_s–t fit may be induced. Nevertheless, this error could be minimized at higher magnetic fields, as the moments would be close to saturation. Therefore, the proposed model can be improved at higher magnetic fields. It is worth noting that, for low thickness films (Figure 3a,e), the saturation magnetization remains low compared to 3.58 μ_B/f.u. expected for isolated Pr^{3+} ions, suggesting that there is still a small fraction of antiferromagnetic (AFM) interaction in the thinner films.

Remarkably, a similar trend in H_c and M_s was also observed for ferrite thin films, which likely indicated a change in the magnetization spin axis, in addition to a reorientation of the domains above critical thickness [28, 29]. In PVO thin films, however, a strong paramagnetic response for thinner films is indicative of dead layer at the surface of films, which consists isolated Pr^{3+} atoms. In addition, a decrease of M_s with increase in film thickness is also evidenced by a decrease in the proportion of the paramagnetic phase. Likewise, the increase of H_c with increase of film thickness could be related to the increase in the density of pinning sites due to increase in the number of domains, and/or domain boundaries. Indeed, due to a partial strain-relaxation, the film could energetically favor multiple domains, as shown earlier [10]. For thick PVO films, the magnetization and coercive field approach a nominal value, meaning that the magnetic contribution from each layer is static, and independent of film thickness. Nevertheless, the magnetization remains lower than the bulk value ($\sim$ 0.6 – 0.7 μ_B/ f.u.) for thick films, and may be related to the presence of V^{4+} / V^{5+}, which can affect the electron hopping, and thus suppress the magnetization considerably.

Further magnetic analyses were carried out by performing magnetic measurements as a function of temperature T. For clarity, only Field Cooled (FC) measurements are shown in Fig. 4(a) and 4(c) for LSAT and LAO substrate, respectively. On the LSAT substrate, PVO films show three distinct anomalies at temperatures T_N, T_{SO2} and T_{SO3} (Fig. 4(a)) while sweeping the temperature from 300 K to 10 K (further confirmed by plotting dM/dT and $\chi^{-1}(T)$). The rising signal at temperature T_N shows the onset of G-type spin ordered state of the vanadium moments, where these moments align antiferromagnetically (|| to $[001]_o$-

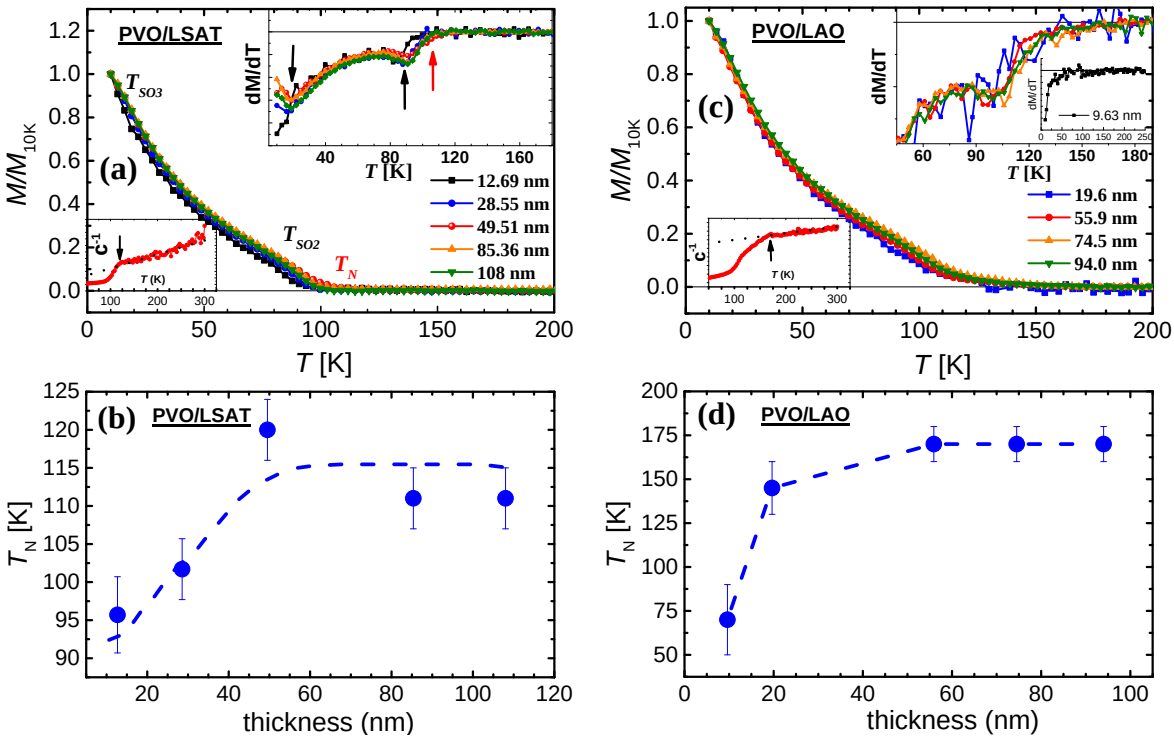

Figure 4: Normalized magnetization measurements for a series of $PrVO_3$ films grown on top of (a) LSAT, and (c) LAO substrate, obtained at $H_{||} = 50$ Oe, displaying different transitions at T_{SO1}, T_{SO2} and T_{SO3}. The inset is dM/dT for respective substrates. (b) T_N (T_{SO1}) as a function of film thickness for (b) PVO/LSAT, (d) PVO/LAO films. The dashed lines are only guide to the eyes.

axis) along the three crystal axis directions *i.e.* *in-plane* and *out-of-plane*. While for bulk $PrVO_3$, the transition at T_N was previously ascribed to the onset of a C-type SO of the canted vanadium moments [26, 30], for epitaxial $PrVO_3$ thin films, the substrate-induced strain results in a G-type SO, as evidenced by the DFT calculations [13]. The T_N displayed by PVO films on LSAT substrates is clearly shown in the inset of Fig. 4(a), and plotted as a function of film thickness in Fig. 4(b). This depicts the tunability of T_N in the range of 25 K for PVO films grown on LSAT substrates by varying film thickness. Moreover, PVO films exhibit additional magnetic features at temperature T_{SO2} and T_{SO3}, established by two kinks in MT (in dM/dT as well) at $\sim$ 90 K and 20 K respectively (Fig. 4(a)). These orderings are however absent in the bulk PVO, but have been manifested by RVO_3 with smaller R size, *eg.* $DyVO_3$, $TbVO_3$ and so on [31–33]. The origin of the magnetic feature at T_{SO2} have two alternative explanations. First, it might be due to magnetic polarization of

the praseodymium sublattice in the presence of exchange field produced by the vanadium moments, via Pr-V exchange, resulting in a ferrimagnetic structure [33]. Second, it could be due to the reorientation of the vanadium spin configuration from G-type to C-type, where V^{3+} spins are staggered in the *ab-plane* and aligned ferromagnetically along c axis. Finally, the transition at T_{SO3} might represent the onset of ferromagnetic (FM) ordering of Pr sublattice, and/or an AFM coupling between Pr^{3+} 4f and V^{3+} 3d moments. Although the Pr^{3+} moments are canted, giving then rise to a finite magnetic moment ($\sim$ 1.1 μ_B), as explained by *Reehuis et. al.* for $Pr_{1-x}Ca_xVO_3$ and bulk RVO_3 (R = *Ce, Dy, Ho, Er*) [31–34]. Remarkably, by comparing the soft magnetic component that was observed in *MH* measurements at temperature $T \leq 20$ K, and the magnetic feature at $T_{SO3} \sim 20$ K, we proposed earlier [10] that, the soft magnetic component could arise from the Pr-V AFM interaction.

Alike PVO films on LSAT substrates, the PVO films on LAO substrates show an abrupt increase in T_N with increase in film thickness and approach a nominal value for the thicker films (Fig. 4(d)). Moreover, it is observed that the transition at T_{SO2} is present only for thicker films, and appear imperceptible for thinner films ($t < 55$ nm) (see inset of Fig. 4(c)). This suggests a possible vanadium spin reorientation solely in the thicker PVO films. Similarly, we observed a clear magnetic feature at T_{SO3} only for the thicker PVO/LAO films, and perhaps related to a different strain states between thinner and thicker films. Notably, the T_N of PVO films decreases with the decrease of film thickness, which is in contrast to the fact that "*the compressive strain enhances the magnetic exchange interactions in PVO films, leading to an increase of* T_N". This discrepancy could be account for the absence of T_{SO2} and T_{SO3} for the thinner PVO films, producing different magnetic ground states, and may be a change in the spin configuration, which, further, are arranged in a way as to decrease the exchange interaction between V-V neighbouring sites, and thus lowering T_N of thinner PVO films. Interestingly, for thinner PVO/LAO films, the soft magnetic component in the *MH* hysteresis loop was seen to persists up to $T \sim 80$ K, meaning that the Pr - V interaction is significantly enhanced for the LAO substrate, in agreement with our previous observations [10]. This enhancement is possibly related to the presence of higher strain states in PVO/LAO films, which raises the degree of Pr-V interaction in the same way as V-V interaction (T_N).

Finally, we have explored the possibility to reduce the film surface by capping it with few

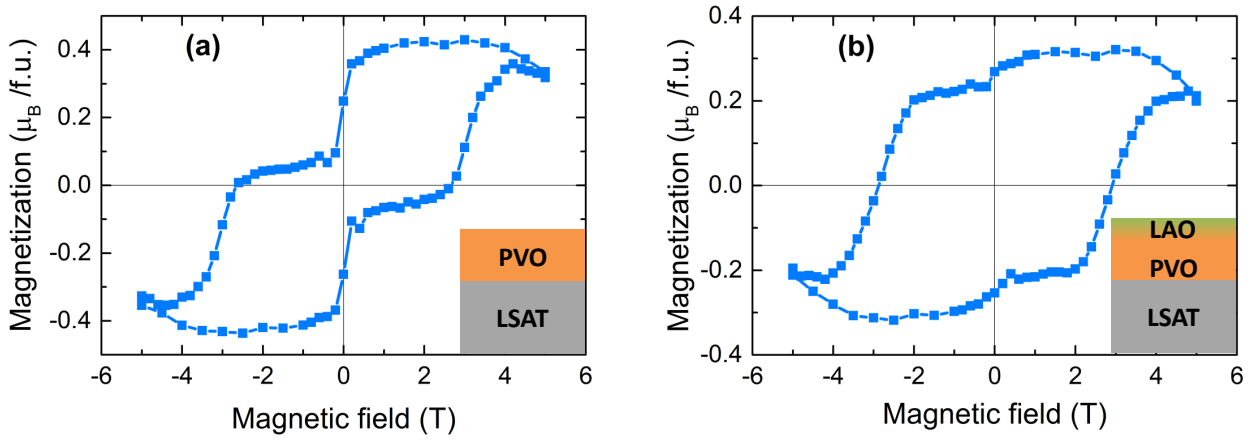

Figure 5: Magnetic hysteresis cycles at 20 K of a $\sim$ 50 nm PVO/LSAT film uncapped (a), and capped with $\sim$ 8 nm thick LAO (b).

layers of LAO. The capping of PVO film surface with a reducing material LAO essentially decreases the formation of V^{4+} / V^{5+} at surface, and thus minimizes the contribution of dead-layer. Following this, we capped PVO film with $\sim$ 8 nm of LAO grown in the same deposition condition in PLD. Fig. 5 illustrates magnetic hysteresis loops of an approximately 50 nm PVO thin film at $T = 20$ K, with and without capping layer. Fig. 5(b) shows a clear improvement of the canted AFM properties of PVO capped with LAO, with a higher remanent magnetization, lower saturation magnetization, and larger H_c. More importantly, the soft magnetic component concomitant with the dead layer is strongly reduced.

In conclusion, we have investigated the effect of film thickness on the structural parameters (*in-plane* and *out-of-plane*) and magnetic properties of compressively-strained $PrVO_3$ (PVO) thin films grown on (La,Sr)(Al,Ta)O_3 (LSAT) (100) (lattice misfit $\sim$ 0.8 %) and $LaAlO_3$ (LAO) (100) (lattice misfit $\sim$ 2.9 %) substrates, and evidenced a *dead layer* of $t \sim$ 4–6 nm for both sample series. The less strained PVO/LSAT films ($\epsilon_{110} \sim 1.4$ % for $t \sim$ 50 nm) show highest $T_N \sim 120$ K, lower than bulk value *i.e.* 130 K. On the other hand, the T_N of highly strained PVO/LAO films ($\epsilon_{110} \sim 2.5$ % for $t \sim 50$ nm) raises up to $\sim$ 170 K, way above its counterpart bulk value. In addition, we have observed an increase in H_c and decrease in M_s with increase in film thickness for both substrates, and explained by the reduction in the proportion of paramagnetic phase. A model based on *dead layer* is used to quantify the salient origin of the large paramagnetic M_s for thinner PVO films. Finally, we

have attempted to cap the PVO film with $\sim$ 8 nm LAO film, in order to partially diminish the excess oxygen at the interface with PVO, and recover the magnetic properties related to the pure PVO. These observations suggest that the film thickness can be used to tune the strain/lattice deformation and thus functional properties in PVO thin films, and should be considered for other epitaxial perovskite thin films.

Acknowledgments

The authors thank F. Veillon for his valuable experimental support. The authors also thanks to S. Froissart for the AFM support and L. Gouleuf for technical support. This work is supported by Region Normandie, by french ANR POLYNASH (ANR-17-CE08-0012) and Labex EMC3. D. K. received his fellowship from Region Normandie.

---

[1] J.H. Haeni, P. Irvin, W. Chang, R. Uecker, P. Reiche, Y.L. Li, S. Choudhury, W. Tian, M.E. Hawley, B. Craigo, A.K. Tagantsev, X.Q. Pan, S.K. Streiffer, L.Q. Chen, S.W. Kirchoefer, J. Levy, and D.G. Schlom, Nature 430, 758 (2004).

[2] H. Meley, Karandeep, L. Oberson, J. de Bruijckere, D.T.L. Alexander, J.-M. Triscone, P. Ghosez, and S. Gariglio, APL Materials 6, 046102 (2018).

[3] Shin-Pei Matsuda, Seiji Takeuchi, Atsuko Soeta, Toshiya Doi, Katsuzou Aihara and Tomoichi Kamo, Japanese Journal of Applied Physics, 29, 1781 (1990).

[4] N.F. Mott, Metal-Insulator Transitions (Taylor and Francis, London,1990).

[5] J.-S. Zhou, J.B. Goodenough, J.-Q. Yan, and Y. Ren, Physical Review Letters 99, 156401 (2007).

[6] D. Bizen, K. Nakatsuka, T. Murata, H. Nakao, Y. Murakami, S. Miyasaka, and Y. Tokura, Physical Review B 78, 224104 (2008).

[7] A.T. Zayak, X. Huang, J.B. Neaton, and K.M. Rabe, Physical Review B 74, 094104 (2006).

[8] Z. Fan, J. Wang, M.B. Sullivan, A. Huan, D.J. Singh, and K.P. Ong, Scientific Reports 4, 4631 (2015).

[9] K. J. Choi, M. Biegalski, Y. L. Li, A. Sharan, J. Schubert, R. Uecker, P. Reiche, Y. B. Chen, X. Q. Pan, V. Gopalan, L.-Q. Chen, D. G. Schlom, C. B. Eom, Science 306, 1005 (2004).

[10] D. Kumar, A. David, A. Fouchet, A. Pautrat, J. Varignon, C.U. Jung, U. Lüders, B. Domengès, O. Copie, P. Ghosez, and W. Prellier, Physical Review B 99, 224405 (2019).

[11] M.H. Sage, G.R. Blake, C. Marquina, and T.T.M. Palstra, Physical Review B 76, 195102 (2007).

[12] S. Miyasaka, Y. Okimoto, M. Iwama, and Y. Tokura, Physical Review B 68, 100406 (2003).

[13] O. Copie, J. Varignon, H. Rotella, G. Steciuk, P. Boullay, A. Pautrat, A. David, B. Mercey, P. Ghosez, and W. Prellier, Advanced Materials 29, 1604112 (2017).

[14] K.I. Kugel and D.I. Khomskii, Zh. Eksp. Teor. Fiz. 64, 1429 (1973).

[15] O. Copie, H. Rotella, P. Boullay, M. Morales, A. Pautrat, P.-E. Janolin, I.C. Infante, D. Pravathana, U. Lüders, and W. Prellier, Journal of Physics: Condensed Matter 25, 492201 (2013).

[16] C.-J. Cheng, C. Lu, Z. Chen, L. You, L. Chen, J. Wang, and T. Wu, Applied Physics Letters 98, 242502 (2011).

[17] S. Valencia, L. Balcells, B. Martínez, and J. Fontcuberta, Journal of Applied Physics 93, 8059 (2003).

[18] P. Kaur, K.K. Sharma, R. Pandit, R.J. Choudhary, and R. Kumar, Applied Physics Letters 104, 081608 (2014).

[19] K. Yoshimatsu, T. Okabe, H. Kumigashira, S. Okamoto, S. Aizaki, A. Fujimori, and M. Oshima, Physical Review Letters 104, 147601 (2010).

[20] T.M. Dao, P.S. Mondal, Y. Takamura, E. Arenholz, and J. Lee, Applied Physics Letters 99, 112111 (2011).

[21] A. Biswas and Y.H. Jeong, Journal of Applied Physics 117, 195305 (2015).

[22] J. Scola, P. Boullay, W. Noun, E. Popova, Y. Dumont, A. Fouchet, and N. Keller, Journal of Applied Physics 110, 043928 (2011).

[23] J. Scola, W. Noun, E. Popova, A. Fouchet, Y. Dumont, N. Keller, P. Lejay, I. Sheikin, A. Demuer, and A. Pautrat, Physical Review B 81, 174409 (2010).

[24] S. Liang, J.R. Sun, J. Wang, and B.G. Shen, Applied Physics Letters 95, 182509 (2009).

[25] R. Aeschlimann, D. Preziosi, P. Scheiderer, M. Sing, S. Valencia, J. Santamaria, C. Luo, H. Ryll, F. Radu, R. Claessen, C. Piamonteze, and M. Bibes, Advanced Materials 30, 1707489 (2018).

[26] F. Wang, J. Zhang, P. Yuan, Q. Yan, and P. Zhang, Journal of Physics: Condensed Matter

328 12, 3037 (2000).
329 [27] U. Aschauer, R. Pfenninger, S.M. Selbach, T. Grande, and N.A. Spaldin, Physical Review B
330 88, 054111 (2013).
331 [28] X. Zhou, Z. Wang, S. Ge, D. Wang, J. Yu, and D. Yao, Physica Status Solidi (A) 211, 2839
332 (2014).
333 [29] F. Zhang, S. Ge, Z. Wang, X. Zhou, G. Wang, Z. Yu, and F. Li, Journal of Alloys and
334 Compounds 506, 109 (2010).
335 [30] M.H. Sage, G.R. Blake, C. Marquina, and T.T.M. Palstra, Physical Review B 76, 195102
336 (2007).
337 [31] M. Reehuis, C. Ulrich, K. Prokeš, S. Mat'aš, J. Fujioka, S. Miyasaka, Y. Tokura, and B.
338 Keimer, Physical Review B 83, 064404 (2011).
339 [32] M. Reehuis, C. Ulrich, P. Pattison, B. Ouladdiaf, M.C. Rheinstädter, M. Ohl, L.P. Regnault,
340 M. Miyasaka, Y. Tokura, and B. Keimer, Physical Review B 73, 094440 (2006).
341 [33] M. Reehuis, C. Ulrich, P. Pattison, M. Miyasaka, Y. Tokura, and B. Keimer, The European
342 Physical Journal B 64, 27 (2008).
343 [34] M. Reehuis, C. Ulrich, P.M. Abdala, P. Pattison, G. Khaliullin, J. Fujioka, S. Miyasaka, Y.
344 Tokura, and B. Keimer, Physical Review B 94, 104436 (2016).